Arch. Pharm. Res. (2015) 38:534–542
DOI 10.1007/s12272-014-0464-8

Archives of Pharmacal Research
www.springer.com/12272

RESEARCH ARTICLE

Enhanced skin permeation of 5α-reductase inhibitors entrapped into surface-modified liquid crystalline nanoparticles

Thiagarajan Madheswaran · Rengarajan Baskaran · Pasupathi Sundaramoorthy · Bong Kyu Yoo

Received: 13 May 2014 / Accepted: 25 July 2014 / Published online: 2 August 2014

Abstract The objective of this study is to enhance skin permeation of finasteride and dutasteride for the treatment of androgenetic alopecia using surface-modified liquid crystalline nanoparticle (sm-LCN) dispersion. LCN entrapped with the drugs was prepared by using monoolein as a liquid crystal former, and surface modification was performed by treatment of the LCN dispersion with same volume of 1 % v/v acetic acid solution containing chitosan. Physicochemical properties of the LCN's were studied with regard to particle size, polydispersity index, zeta potential, and release of the drugs. Skin permeation of drugs entrapped into the LCN and sm-LCN was investigated with porcine abdominal skin using Franz diffusion cell. Cytotoxicity of the LCN's was also studied using human skin keratinocytes. The particle size and zeta potential of the LCN were 197.9 ± 2.5 nm and −20.2 ± 1.9 mV, respectively, and sm-LCN showed slightly bigger size and positive zeta potential due to the presence of thin coating on the surface of the nanoparticles. Compared to LCN, sm-LCN resulted in significantly enhanced skin permeation of the drugs whereas in vitro release was significantly reduced. Cell viability as a measure of cytotoxicity was above 80 % up to 20 μg/ml concentration of both LCN and sm-LCN. In conclusion, sm-LCN may provide a strategy to maximize therapeutic efficacy minimizing unwanted systemic side effects associated with the use of the drugs for the treatment of androgenetic alopecia.

Keywords Liquid crystalline nanoparticles · Chitosan · Finasteride · Dutasteride · Skin permeation

Introduction

5α-reductase is a major enzyme responsible for the conversion of testosterone to more potent dihydrotestosterone (DHT) and involved in the pathophysiology of androgenetic alopecia (AGA) (Azzouni et al. 2013). It increases DHT level in scalp skin and causes gradual miniaturization of hair follicles resulting in patterned hair loss (Banka et al. 2013; Inui and Itami 2013). In this regard, 5α-reductase inhibitors such as finasteride (FNS) and dutasteride (DT) are used in the treatment of male pattern baldness or AGA (Blumeyer et al. 2011). Specifically, FNS inhibits type II 5α-reductase whereas DT inhibits both type I and II of the enzyme with three times greater potency compared to FNS (Gupta and Charrette 2014). By lowering the DHT level in scalp skin, 5α-reductase inhibitors increase hair follicle population in the anagen phase, and therefore, inhibit the progression of hair loss (Inui and Itami 2011; Van Neste et al. 2000). Although 5α-reductase inhibitors have been proved effective in the treatment of AGA, oral administration of these medications also inhibits DHT level throughout the body. Impotence, decreased libido, and ejaculation disorder are typical examples of the side effects associated with long-term use of the drugs by oral route (Gupta and Charrette 2014; Gur and Kadowitz 2013; Mysore 2012) To overcome these limitations, it was hypothesized that topical application would be a route of

R. Baskaran: Contributed same as first author.

T. Madheswaran
College of Pharmacy, Yeungnam University, 214-1 Dae-dong, Gyeongsan 712-749, South Korea

R. Baskaran · P. Sundaramoorthy · B. K. Yoo (✉)
College of Pharmacy, Gachon University, 191 Hambakmoero, Incheon 406-799, South Korea
e-mail: byoo@gachon.ac.kr

choice to deliver 5α-reductase inhibitors (Valente Duarte de Sousa and Tosti 2013; Hajheydari et al. 2009).

However, development of efficient transdermal vehicle has been restricted by natural barrier function exerted by stratum corneum (SC) (Jepps et al. 2013). Numerous nanocarrier systems such as microemulsion, liposome, polymeric nanoparticle, solid lipid nanoparticle, and LCN have been studied to infiltrate the barrier layer (Cevc and Vierl 2010; Zhang and Michniak-Kohn 2011; Prow et al. 2011; Lapteva and Kalia 2013). Among those, monoolein (MO)-based LCN has gained attention because of its unique structural properties that favors permeation through SC (Lapteva and Kalia 2013). MO-based liquid crystalline cubic phase is formed via self-assembly of melted MO in the presence of water at specified temperature (Kulkarni et al. 2011; Mulet et al. 2013). This liquid crystalline cubic phase can be formulated into LCN dispersion by sonication or high pressure homogenization along with addition of polymeric surfactants (Guo et al. 2010).

Surface modification of nanoparticulate system with mucoadhesive cationic polymer such as chitosan (CHI) has been often considered a strategy to enhance topical delivery. Owing to its positive charge, it adheres to the negatively charged mucous layer, and therefore, enhances the permeation of the drugs (Ridolfi et al. 2012). Recently, researchers have shown that the nanoparticulate system can be surface-modified using CHI (Svensson et al. 2008; Chang et al. 2012). However, there have been no reports on the effect of surface modification of LCN towards skin delivery of FNS and DT. Thus, we have hypothesized that surface modification of MO-based LCN using CHI may improve the skin permeation of FNS and DT for the treatment of AGA.

The main aim of this study was to investigate the effect of surface modification of MO-based LCN on the skin permeation of FNS and DT. Characterizations of the LCN's and release profile of the drugs were also performed. Additionally, we evaluated cytotoxicity of LCN dispersion using human skin keratinocyte cell line.

Materials and methods

Materials

MO was received as a gift from Danisco Japan (Tokyo, Japan). FNS and DT were kindly donated from Dong-A Pharmaceutical Co, South Korea. Poloxamer 407 was purchased from BASF (Ludwigshafen, Germany). Chitosan (low molecular weight, Prod. No. 448869) and rhodamine 6 g were obtained from Sigma-Aldrich, Korea. Dialysis membrane was purchased from Spectrum Laboratories Inc (Rancho Dominguez, California, USA). All other chemicals were of analytical grade and used without further purification.

Table 1 Compositions of LCN and sm-LCN

Formulation code	MO	P 407	CHI	FNS	DT
LCN	4.00	0.40	–	0.10	0.05
sm-LCN 1.25	4.00	0.40	0.05	0.10	0.05
sm-LCN 2.5	4.00	0.40	0.10	0.10	0.05
sm-LCN 5	4.00	0.40	0.20	0.10	0.05
sm-LCN 7.5	4.00	0.40	0.30	0.10	0.05

CHI chitosan, *DT* dutasteride, *FNS* finasteride, *LCN* liquid crystalline nanoparticles, *MO* monoolein, *P 407* poloxamer 407, *sm-LCN* surface-modified liquid crystalline nanoparticle

Preparation of LCN and sm-LCN

LCN was prepared by ultrasonication method as described previously (Madheswaran et al. 2013a). The compositions of the formulation are shown in Table 1. Briefly, MO and poloxamer 407 (P 407) were melted at 45 °C in a glass vial, and FNS and DT were added and dissolved with magnetic stirring. Distilled water heated at the same temperature was added dropwise to the mixture and vortexed for 1 min to form liquid crystalline cubic phase followed by sonication for 15 min using bath type sonicator (Cole-Parmer Ultrasonic 8893, USA) at 42,000 Hz to prepare finely dispersed LCN dispersion. The lipid content of the LCN dispersion was 40 mg/ml and lipid to surfactant ratio was 90:10 by weight. Blank LCN without the drugs were also prepared for comparison. Surface modification of the LCN was performed by method described elsewhere (Svensson et al. 2008). Briefly, the LCN dispersion was mixed with same volume of CHI solution in 1 % acetic acid and stirred for 30 min. The amount of CHI with regard to MO was varied from 1.25 to 7.5 % by weight.

Characterization of the LCN and sm-LCN

Particle size distribution, polydispersity index and zeta potential

The particle size distribution, polydispersity index and zeta potential of the LCN and sm-LCN were determined by dynamic light scattering using Zetasizer Nano S90 (Malvern, Worcestershire, UK) at fixed angle of 90°. The dispersion was suitably diluted with distilled water (18.2 MΩ cm^{-1}) and measured at 25 °C. Data were collected after 2 min equilibration time and averaged over five measurements.

Morphology

Morphology of LCN and sm-LCN was visualized by transmission electron microscope (TEM, Hitachi 7600,

Japan) and atomic force microscope (AFM, Veeco Nano-Scope IV Multimode AFM, Plainview, NY, USA). For TEM, a drop of diluted sample was placed in carbon-coated grid and excess sample was removed with filter paper after 5 min. One drop of 2 % phosphotungstic acid solution was added to negatively stain the nanoparticle for contrast enhancement followed by air-drying at room temperature for 5 min. TEM images were taken at an accelerating voltage of 100 kV. For AFM, samples were suitably diluted with distilled water and then dropped onto mica plates followed by morphological evaluation in tapping mode at scan speed of 1 Hz.

Entrapment efficiency (EE)

Ultrafiltration method was used to determine EE of the two drugs as described elsewhere (Madheswaran et al. 2013a). Sample (1 ml) was centrifuged at 2,500×*g* for 15 min using Amikon Ultra-4 (MWCO: 10,000 g/mole, Billerica, MA, USA), and the filtrate containing free drugs was analyzed by HPLC described below. Preliminary experiments were performed for the optimization of ultracentrifugation, which proved 2,500 × *g* for 15 min was sufficient for separation of the unentrapped drugs from entrapped drug. Total amount of the drugs in the sample was measured using HPLC after destruction of the liquid crystalline cubic phase by dilution with methanol (× 20). EE was calculated by the following equation:

$$\text{EE}\ (\%) = 100 \times (\text{D}_\text{t} - \text{D}_\text{f})/\text{D}_\text{t},$$

where D_t and D_f are the amount of total and free (unentrapped) drug in the sample, respectively.

HPLC analysis

FNS and DT were assayed by HPLC system (Shimadzu Corp, Japan) equipped with LC 20 AD pump and SPD 20A UV–VIS detector at 210 nm. The column used was Inertsil ODS-3 (4.6 × 150 mm, GL Science, Japan) and mobile phase consisted of mixture of acetonitrile and water (60:40 v/v, pH adjusted to 2.8 with orthophosphoric acid). Ibuprofen was used as internal standard and injection volume was 20 µl with flow rate of 1 ml/min. HPLC assay validation was performed five times a day for five consecutive days in the range of 0.05–50 µg/ml concentration of the drugs.

In vitro drug release

Release of FNS and DT from LCN and sm-LCN was evaluated in Franz diffusion cell using artificial membrane made of regenerated cellulose with MWCO 10,000 g/mole (Spectra/Por®, Rancho Dominguez, California, USA). The membrane was mounted between donor and receptor compartments, and 500 µl of the sample was applied evenly on the donor compartment. The diffusion surface area was 2.1 cm^2 and receptor compartment volume was 10 ml. The release medium used was 20 % v/v ethanol in phosphate buffer saline (pH 7.4) to ensure sink condition and maintained at 32 ± 0.5 °C with magnetic stirring. Aliquots of the sample (500 µl) were withdrawn at fixed time intervals (1, 2, 3, 6, 12, and 24 h) from the receptor compartment and replaced with fresh medium. The samples were then analyzed for FNS and DT concentration using HPLC. Each experiment was performed in triplicate.

In vitro skin permeation

In vitro skin permeation studies were performed with porcine skin using Franz diffusion cell. Porcine skin was obtained from a local abattoir house and carefully dissected to ensure complete removal of the subcutaneous fat, and then, dermatomed to 700–800 µm and stored at −20 °C. The skin was mounted in Franz diffusion cell (diffusion area: 2.1 cm^2) with SC layer facing towards donor compartment and dermis layer facing towards receptor compartment, which was filled with 10 ml of medium containing 20 % v/v ethanol in the phosphate-buffered saline. Ethanol was used to ensure sink condition of receptor compartment during the skin permeation study. The medium was under constant stirring at 400 rpm and held at a 32 °C. Five hundred microliters (500 µl) of sample (equivalent to 500 µg of FNS and 250 µg of DT) were applied onto the skin and sealed with Parafilm® to prevent water evaporation. Samples from receptor compartment were collected at predetermined time interval (1, 2, 3, 6, 12, and 24 h) and replaced with the same volume of the fresh medium. Amount of the drugs permeated was determined by HPLC mentioned above. Control sample was also prepared and examined with FNS and DT dissolved into 20 % v/v ethanol in the phosphate-buffered saline.

The steady-state flux (J_{ss}, µg cm^{-1} h^{-1}) was calculated from the slope of linear regression interpolation of the cumulative amount of the drug permeated per unit area (Q, µg cm^{-1}) as a function of time, and lag time (T_L, h) was taken as intercept of X-axis. The slope and intercept were derived using GraphPad Prism® v.4.00 software. The permeability coefficient was calculated by the following equation:

$$\text{K}_\text{p} = \text{Jss}/[(\text{DC}_\text{i} + \text{DC}_\text{f})/2],$$

where DC_i and DC_f are the initial and final concentration of the donor compartment, respectively.

Molecular organization of lipid matrix in SC

The effect of LCN and sm-LCN on the molecular organization of lipid matrix in SC was investigated by attenuated total reflectance Fourier-transform infrared spectroscopy (ATR-FTIR) using porcine skin. Porcine skin was treated with same conditions as in vitro skin permeation study during 6 h for the FTIR analysis. And then, spectrum was recorded by FTIR spectrophotometer equipped with ATR (Tensor 27, Bruker Optics, Germany) containing photovoltaic mercury cadmium telluride (MCT) detector in the wave number range of 4,000–400 cm^{-1} by placing SC layer exposed to surface of ZnSe crystal at 25 °C. Spectral data were analyzed using software OPUS 6.5.

Cytotoxicity of LCN and sm-LCN

Cytotoxicity of LCN and sm-LCN was carried out with human skin keratinocytes (HaCaT cells) using MTT (3-(4, 5-dimethylthiazol-2-yl)-2, 5-diphenyl tetrazolium bromide) assay. HaCaT cells were seeded in a 96-well plate at a density of 4×10^4 cells/well in DMEM medium supplemented with 10 % fetal bovine serum and incubated for 24 h to allow cell adherence. The cells were then treated with different concentration of LCN's. After 24 h, the medium containing LCN's was removed and 100 µl of MTT solution (0.5 mg/ml) was added to each well and cells were incubated for 4 h at 37 °C in a humidified environment of 5 % CO_2 atmosphere. Then, the medium was removed and 100 µl DMSO was added to dissolve the formazan crystals formed by living cells. The plate was shaken for 5 min the absorbance was measured at 570 nm using a microplate reader. Cell viability was calculated by the following equation:

$$\text{cell viability } (\%) = 100 \times A_s/A_0,$$

where A_s is the absorbance of the cells treated with medium containing LCN or sm-LCN and A_0 is the absorbance of the cells treated with the medium only. All experiments were repeated six times.

Cytotoxicity of each ingredient of the LCN was also tested. MO was melted and dispersed in distilled water with the aid of sonication for 15 min, and CHI was dissolved into 1 % acetic acid solution. P 407 was directly dissolved into distilled water. Samples containing each ingredient were appropriately diluted with the medium and tested by exactly same procedure as cytotoxicity test for LCN's.

Statistical analysis

All the data obtained were analyzed by Student's *t* test using Microsoft Office Excel 2010. Data are presented as mean ± standard deviation. A value of $p < 0.05$ was considered statistically significant.

Results

The particle size and polydispersity index of LCN and sm-LCN measured by dynamic light scattering are shown in Table 2. Mean particle size of the blank and drug-loaded LCN was 190.1 ± 3.4 and 197.9 ± 2.5 nm, respectively, with polydispersity index of less than 0.3. Mean particle size of sm-LCN was found to be significantly bigger than LCN in proportion to the amount of CHI used for surface modification ($p < 0.01$). When CHI was used with 7.5 % of MO, it was 248.6 ± 6.5 nm. The size increase in proportion to the amount of CHI indicates that the increment is due to CHI coated on the surface of LCN. Reversed charge in zeta potential further supports that protonated amino groups of the CHI molecules are well anchored on the negatively charged surface of the LCN. Zeta potential was −20.2 ± 1.9 mV in the drug-loaded LCN and it was +48.5 ± 1.2 mV in the drug-loaded sm-LCN 7.5. Entrapment of FNS and DT slightly affected particle size and zeta potential of the LCN's prepared, but the change was not significant.

TEM and AFM images confirmed the results of dynamic light scattering study, revealing monodispersed nanoparticles in LCN dispersion and core–shell structure in sm-LCN dispersion (Figs. 1 and 2). Morphology of the particles was spherical and multifaceted geometry, and the size of the particles was less than 300 nm which is consistent with the dynamic light scattering characterization. In case of sm-LCN, dense black core represents the LCN particle while less-stained grayish outer layer is attributed to the presence of the CHI shell confirming surface modification of LCN. Furthermore, AFM provided the evidence of the stability of LCN and sm-LCN withstanding the multi-dimensional scanning forces and preserving their surface topography.

Figure 3 shows the release profile of FNS and DT from LCN and sm-LCN. FNS and DT were released in a controlled manner from LCN and sm-LCN. Cumulative amount of the drug released from LCN and sm-LCN 7.5 during 24 h was 38.13 and 32.37 % for FNS, respectively, and it was 5.42 and 3.15 % for DT in the corresponding order. The extent of delaying the release of the drugs was in proportion to the amount of CHI used for the surface modification of the LCN. This result indicates that LCN exerted sustained release of the drugs entrapped into the LCN, and surface modification with CHI further delayed the release of the drugs.

Skin permeation of FNS and DT through the porcine skin was significantly enhanced when the drugs were entrapped into the LCN and sm-LCN (Fig. 4). Cumulative

Table 2 Characterization parameter of LCN and surface-modified LCN

Formulation code	Size (nm)		PDI		Zeta potential (mV)		EE (%)	
	Blank	Drug-loaded	Blank	Drug-loaded	Blank	Drug-loaded	FNS	DT
LCN	190.1 ± 3.4	197.9 ± 2.5	0.22 ± 0.02	0.24 ± 0.03	-19.8 ± 0.7	-20.2 ± 1.9	98.4 ± 0.1	99.1 ± 0.2
sm-LCN 1.25	228.7 ± 2.6**	239.6 ± 3.3	0.25 ± 0.03	0.26 ± 0.02	19.4 ± 1.2	19.8 ± 2.5	98.2 ± 0.1	98.7 ± 0.1
sm-LCN 2.5	238.7 ± 3.8**	250.2 ± 5.3	0.26 ± 0.01	0.28 ± 0.02	21.5 ± 2.1	22.1 ± 3.4	98.5 ± 0.2	99.0 ± 0.2
sm-LCN 5	242.0 ± 3.6**	257.7 ± 3.0	0.33 ± 0.01	0.34 ± 0.02	31.7 ± 1.8††	34.9 ± 2.5††	99.1 ± 0.1	99.1 ± 0.3
sm-LCN 7.5	248.6 ± 6.5**	259.8 ± 7.5	0.31 ± 0.01	0.32 ± 0.5	45.4 ± 3.5††	48.5 ± 1.2††	99.0 ± 0.2	98.9 ± 0.2

Each value represents the mean ± SD ($n = 3$). ** $p < 0.01$ compared to LCN, †† $p < 0.01$compared to sm-LCN 1.25

DT dutasteride, *EE* entrapment efficiency, *FNS* finasteride, *LCN* liquid crystalline nanoparticles, *PDI* polydispersity index, *sm-LCN* surface-modified liquid crystalline nanoparticle

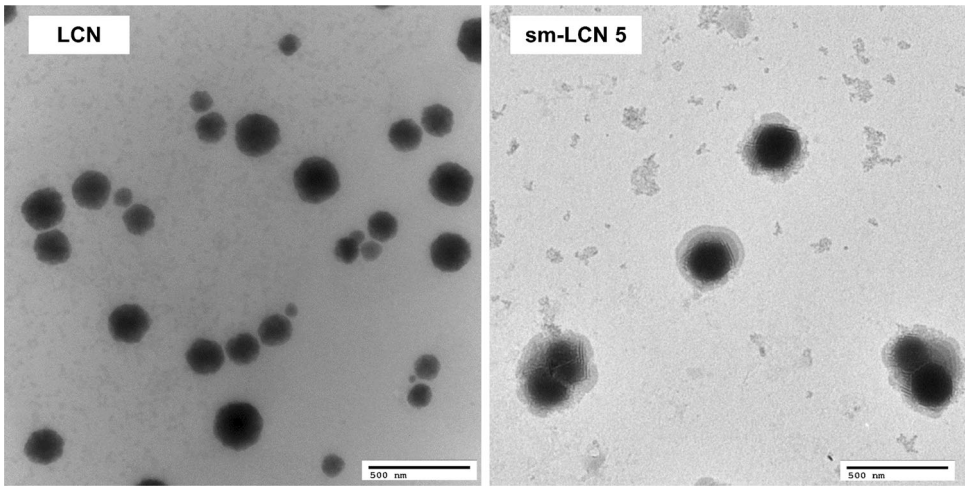

Fig. 1 TEM images of LCN and sm-LCN (*bar* 500 nm). LCN Liquid crystalline nanoparticle, sm-LCN Surface-modified liquid crystalline nanoparticle

amount of FNS permeated through the skin during 24 h was 2.38 ± 0.12 μg/cm^2 in LCN, which is slightly greater than the value observed in the control. However, it was 4.18 ± 0.21 and 9.94 ± 0.72 μg/cm^2 in sm-LCN 1.25 and sm-LCN 7.5, respectively, which accounts for 1.7- and 4.2-fold increase compared to LCN in the corresponding order ($p < 0.01$). Skin permeation of DT in the sm-LCN through the skin was also significantly enhanced and the enhancement was in proportion to the amount of CHI used. The skin permeation profiles of FNS and DT through the porcine skin are depicted in Fig. 4 and the skin permeation parameters are shown in Table 3.

The effect of LCN and sm-LCN on the molecular organization of the lipids matrix in the SC was evaluated using ATR-FTIR spectroscopy. Treatment of porcine skin with the LCNs caused shift of the IR bands for CH_2 asymmetric stretching and CH_2 symmetric stretching towards higher wave number compared to the bands observed when the skin was treated with distilled water (Table 4). On the other hand, band for CH_2 scissoring was shifted to lower wave number and C = O stretching was disappeared by treatment with LCNs. However, there was no difference in the results observed between LCN and sm-LCN.

Figure 5a shows the in vitro cytotoxic effect of LCN and sm-LCN 5 on HaCaT cell lines. The cell viability was above 80 % up to 20 μg/ml of the nanoparticle concentration. There was no significant difference observed in cytotoxicity between LCN and sm-LCN. IC_{50} (50 % inhibition of cell viability) was about 150 μg/ml of the nanoparticle concentration for LCN and sm-LCN formulations. However, each ingredient used to prepare nanoparticle showed no toxic effect on the cell viability even at the highest concentration, i.e., 500 μg/ml (Fig. 5b).

Discussion

Androgen plays a key role in causing miniaturization of hair follicles, resulting in patterned hair loss. In this regard, 5α-reductase inhibitors such as FNS and DT have been used for the treatment of AGA. However, it has been reported that hair loss resumes in later course of FNS therapy which might be due to the specific binding

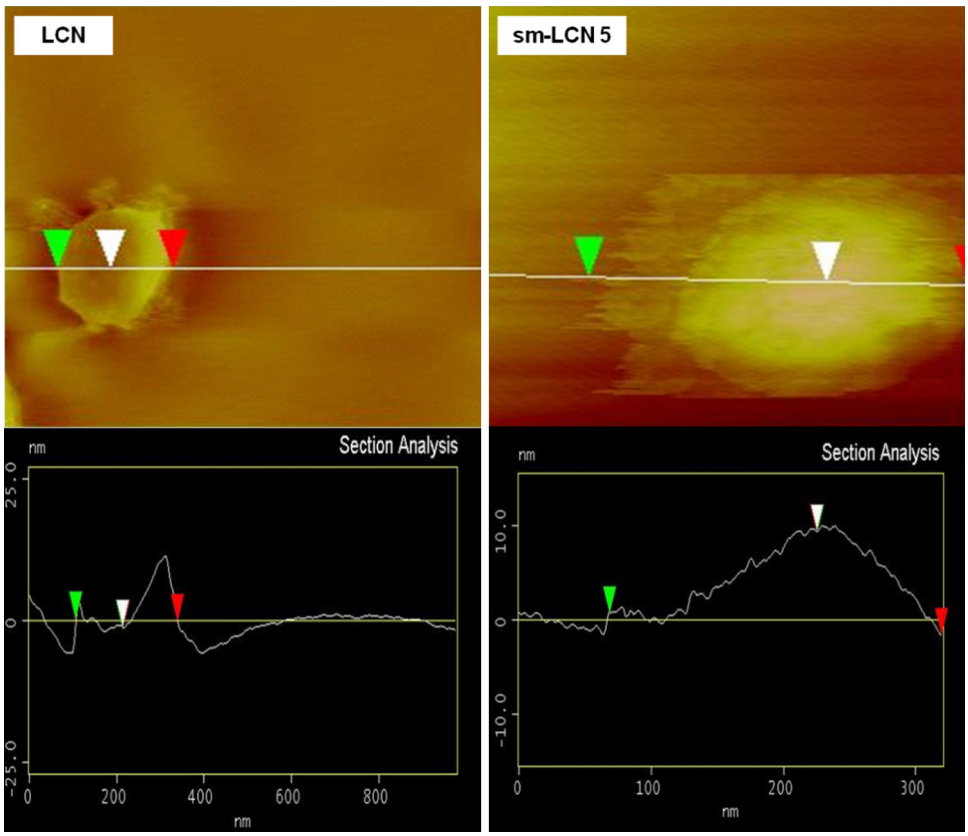

Fig. 2 AFM images of LCN and sm-LCN. LCN Liquid crystalline nanoparticle, sm-LCN Surface-modified liquid crystalline nanoparticle

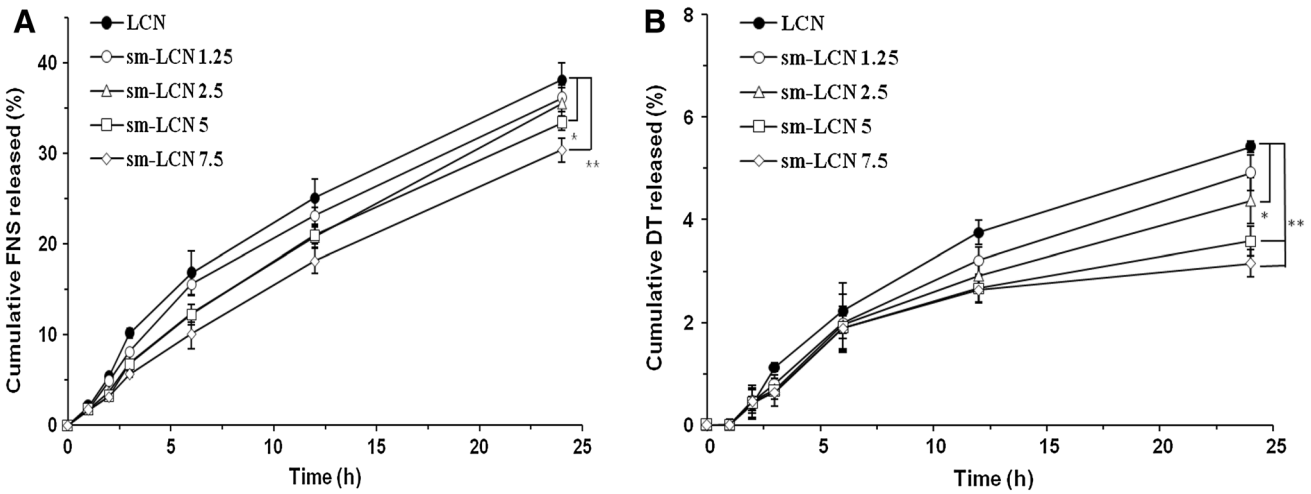

Fig. 3 Cumulative release profile of entrapped drugs from LCN and sm-LCN using Spectra/Por® (MWCO 10,000 g/mol). **a** Release of FNS; **b** Release of DT. Each value represents mean ± SD ($n = 3$). $^{*}p < 0.05$ compared to LCN, $^{**}p < 0.01$ compared to LCN. DT Dutasteride, FNS Finasteride, LCN Liquid crystalline nanoparticle, sm-LCN Surface-modified liquid crystalline nanoparticle

properties of FNS with type II 5α-reductase, indicating the need for concomitant use of a drug with efficacy toward type I 5α-reductase. Recently, Boyapati and her colleague reported that addition of low-dose DT resulted in a dramatic increase of hair density in patients already taking FNS (Boyapati and Sinclair 2013).

However, both drugs have common persistent sexual side effects when used via systemic route. In this regard, topical application of 5α-reductase inhibitors has been proposed as an alternative strategy to avoid drug-related side effects (Valente Duarte de Sousa and Tosti 2013; Farshi et al. 2012). In our earlier studies, we have

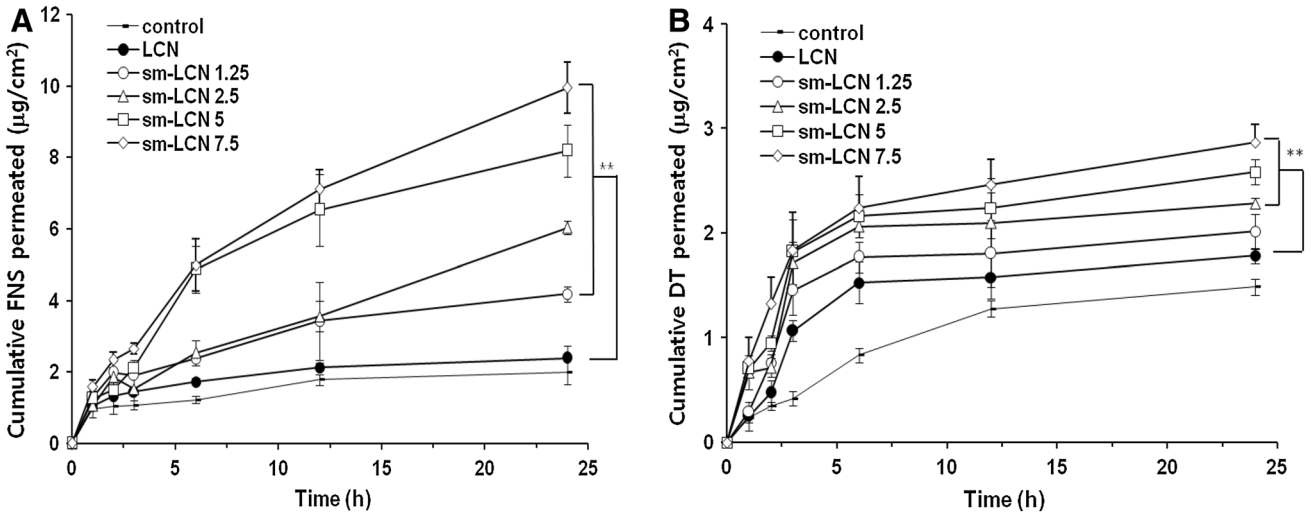

Fig. 4 Cumulative permeation profiles of entrapped drugs from LCN and sm-LCN using porcine skin. **a** Permeation of FNS; **b** Permeation of DT. Each value represents mean ± SD ($n = 3$). $^{**}p < 0.05$ compared to LCN. DT Dutasteride, FNS Finasteride, LCN Liquid crystalline nanoparticle, sm-LCN Surface-modified liquid crystalline nanoparticle

Table 3 Results of skin permeation studies using porcine skin

Formulation code	Permeation parameters							
	J_{ss} (μg cm^{-2} h^{-1})		K_p ($\times 10^{-4}$ cm h^{-1})		T_L (h)		ER	
	FNS	DT	FNS	DT	FNS	DT	FNS	DT
LCN	0.002 ± 0.001	0.002 ± 0.001*	0.040 ± 0.018	0.093 ± 0.010*	1.31 ± 0.31	0.66 ± 0.05	1.14	0.81
sm-LCN 1.25	0.005 ± 0.001*,†	0.002 ± 0.001*	0.112 ± 0.015*†	0.099 ± 0.009*	1.65 ± 0.10	0.06 ± 0.04	2.65	0.86
sm-LCN 2. 5	0.008 ± 0.001**,††	0.003 ± 0.001*	0.198 ± 0.018**††	0.099 ± 0.010*	1.18 ± 0.18	1.11 ± 0.03	4.62	0.86
sm-LCN 5	0.013 ± 0.002*,††	0.004 ± 0.001	0.264 ± 0.039**,††	0.122 ± 0.030	1.67 ± 0.08	1.20 ± 0.09	6.96	1.11
sm-LCN 7.5	0.015 ± 0.001**,††	0.004 ± 0.002†	0.308 ± 0.030**,††	0.127 ± 0.011*,†	1.94 ± 1.22	1.32 ± 0.25	8.11	1.12
control	0.002 ± 0.001	0.002 ± 0.001	0.039 ± 0.008	0.091 ± 0.015	1.22 ± 0.02	0.30 ± 0.08	–	–

Each value represents the mean ± SD ($n = 3$). $^{*}p < 0.05$, $^{**}p < 0.01$ compared to control; $^{\dagger}p < 0.05$, $^{\dagger\dagger}p < 0.01$compared to LCN

DT dutasteride, *ER* enhancement ratio of flux compared to control (FNS dissolved in 20 % v/v ethanol in PBS), *FNS* finasteride, J_{ss} flux, K_p permeation coefficient, *LCN* liquid crystalline nanoparticles, *sm-LCN* surface-modified liquid crystalline nanoparticle, T_L lag time

Table 4 ATR-FTIR Characteristic bands of porcine skin after treatment with LCN dispersions for 6 h

Formulation code	CH_2 asymmetric stretching	CH_2 symmetric stretching	C = O stretching	CH_2 scissoring
Distilled water	2,918.5 ± 0.3	2,850.7 ± 0.2	1,736.9 ± 0.8	1,457.0 ± 0.3
LCN	2,924.2 ± 0.2	2,854.1 ± 0.2	–	1,454.2 ± 0.1
sm-LCN 1.25	2,925.2 ± 0.3	2,854.1 ± 0.2	–	1,455.3 ± 0.2
sm-LCN 2.5	2,925.0 ± 0.1	2,854.1 ± 0.2	–	1,455.1 ± 0.1
sm-LCN 5	2,925.2 ± 0.3	2,855.1 ± 0.2	–	1,454.9 ± 0.2
sm-LCN 7.5	2,925.2 ± 0.5	2,855.2 ± 0.2	–	1,455.2 ± 0.3

Each value represents the mean ± SD ($n = 3$)

LCN liquid crystalline nanoparticles, *sm-LCN* surface-modified liquid crystalline nanoparticle

demonstrated that topical application of MO-based LCN dispersion enhanced transdermal delivery of FNS (Madheswaran et al. 2013a, 2013b). Extending our previous work, we have hypothesized that surface modification of LCN with positively-charged CHI molecules might further enhance transdermal delivery of 5α-reductase inhibitors.

In this study, we successfully prepared sm-LCN by using CHI as a positively-charged coating material on the

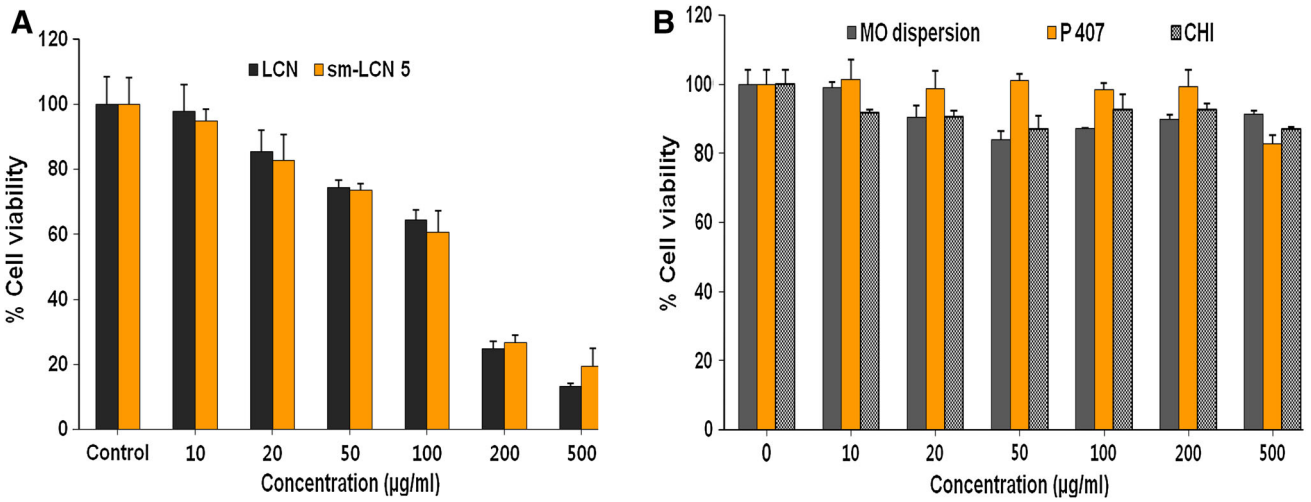

Fig. 5 Cell viability of HaCaT incubated in the presence of nanoparticles (**a**) and each formulation ingredient (**b**). Each value represents mean ± SD ($n = 6$). LCN Liquid crystalline nanoparticles, MO Monoolein, P 407 Poloxamer 407, sm-LCN Surface-modified liquid crystalline nanoparticle

surface of the LCN. Rate and extent in the skin permeation of drugs depend on the physicochemical properties of the vehicles as well as drugs. Lipid layer in the SC contains high ratio of negatively-charged lipids. Therefore, positively-charged LCN formulation may interact with SC by electrostatic attraction and result in better permeation of drugs to the skin (Rojanasakul et al. 1992; Piemi et al. 1999). Our skin permeation study demonstrated that sm-LCN, positively-charged nanoparticle dispersion, was capable of enhancing the rate and extent in the skin permeation of FNS and DT. This finding confirmed the hypothesis that positively-charged LCN enhances transdermal delivery of drugs loaded into it.

In our earlier study, skin permeation of FNS from the MO-based LCN was proportional to the release rate of the drug (Madheswaran et al. 2013a). However, in this study, skin permeation of FNS and DT from the sm-LCN was inversely proportional to the release rate (Figs. 3 and 4). Reason for this opposite result is attributed to the difference in the surface charge of the LCNs tested. In the previous work, the LCN was negatively-charged while the sm-LCN in this study was positively-charged. Taking into account that skin tissues are abundant with negatively-charged lipids, it is likely that the magnitude of the positive charge on the surface of the sm-LCN may exert as a driving force for skin permeation of the drugs entrapped into the nanoparticles. Hence, skin permeation was more affected by the magnitude of positive charge on the nanoparticles than the release of the drug whereas drug release was dependent on the thickness of coating (amount of CHI used). In short, release rate is a rate-limiting factor for skin permeation only when there is no other driving force than concentration gradient. This phenomenon should be taken into consideration when sm-LCN is applied on the skin for iontophoresis.

With regard to in vitro drug release, the release profiles for FNS and DT were strikingly different. Cumulative amount of DT released during 24 h was only about 5 % or less whereas it was about above 30 % for FNS (Fig. 3). This might be attributed to highly lipophilic nature of DT which renders strong interaction with lipid bilayer inside the LCN structure, and therefore, remains bound to LCN for a long time.

Ingredients used for the preparation of LCN in this study were MO, P 407, and CHI which are generally recognized as safe by Food and Drug Administration of US. Therefore, as was expected, no cytotoxicity was observed even at the highest concentration of each ingredient (Fig. 5b). However, LCN prepared with the non-toxic ingredients was shown to be toxic to HaCaT cell lines in dose-dependent manner. This result is consistent with Liu and his colleagues' finding that glycerol monooleate-based LCN were non-toxic only up to 20 μg/ml concentration of the nanoparticles (Liu et al. 2013). Murgia and his colleagues have also noted that monooleate-based LCN displays certain toxicity toward different cell lines whereas liposomal nanoparticles affect cell viability at a much lesser extent (Murgia et al. 2010). Although not elucidated, the cytotoxicity associated with the LCN appears to be due to cellular uptake (internalization) which may trigger various signal transduction pathways in cell membrane (Park et al. 2012). Cellular uptake study of the LCN and sm-LCN is currently ongoing in our lab using fluorescence-activated cell sorter.

In conclusion, surface modification of LCN with CHI resulted in enhanced skin permeation of FNS and DT

entrapped into the nanoparticular vehicle. The enhanced skin permeation of the drugs was driven by positive charge on the surface of the nanoparticles and this finding may provide useful strategy to maximize the therapeutic efficacy toward the affected area minimizing various unwanted side effects associated with oral use of the drugs.

Acknowledgments This work was supported by the Gachon University research fund of 2014-M016.

References

Azzouni, F., N. Zeitouni, and J. Mohler. 2013. Role of 5α-reductase inhibitors in androgen-stimulated skin disorders. *Journal of Drugs in Dermatology* 12: e30–e35.

Banka, N., M. Bunagan, and J. Shapiro. 2013. Pattern hair loss in men: diagnosis and medical treatment. *Dermatologic Clinics* 31: 129–140.

Blumeyer, A., A. Tosti, A. Messenger, P. Reygagne, V. del Marmol, P.I. Spuls, M. Trakatelli, A. Finner, F. Kiesewetter, R. Trüeb, R. Rzany, and U. Blume-Peytavi. 2011. Evidence-based (S3) guideline for the treatment of androgenetic alopecia in women and in men. *Journal der Deutschen Dermatologischen Gesellschaft* 9: S1–S57.

Boyapati, A., and R. Sinclair. 2013. Combination therapy with finasteride and low-dose dutasteride in the treatment of androgenetic alopecia. *Australasian Journal of Dermatology* 54: 49–51.

Cevc, G., and U. Vierl. 2010. Nanotechnology and the transdermal route: a state of the art review and critical appraisal. *Journal of Controlled Release* 141: 277–299.

Chang, D.P., M. Jankunec, J. Barauskas, F. Tiberg, and T. Nylander. 2012. Adsorption of lipid liquid crystalline nanoparticles on cationic, hydrophilic, and hydrophobic surfaces. *ACS Applied Materials and Interfaces* 4: 2643–2651.

Farshi, S., P. Mansouri, and F. Rafie. 2012. A randomized double blind, vehicle controlled bilateral comparison study of the efficacy and safety of finasteride 0.5% solution in combination with intense pulsed light in the treatment of facial hirsutism. *Journal of Cosmetic and Laser Therapy* 87: 193–199.

Guo, C., J. Wang, F. Cao, R.J. Lee, and G. Zhai. 2010. Lyotropic liquid crystal systems in drug delivery. *Drug Discovery Today* 15: 1032–1040.

Gupta, A.K., and A. Charrette. 2014. The efficacy and safety of 5α-reductase inhibitors in androgenetic alopecia: a network meta-analysis and benefit-risk assessment of finasteride and dutasteride. *Journal of Dermatological Treatment* 25: 156–161.

Gur, S., P.J. Kadowitz, and W.J. Hellstrom. 2013. Effects of 5-alpha reductase inhibitors on erectile function, sexual desire and ejaculation. *Expert Opinion on Drug Safety* 12: 81–90.

Hajheydari, Z., J. Akbari, M. Saeedi, and L. Shokoohi. 2009. Comparing the therapeutic effects of finasteride gel and tablet in treatment of the androgenetic alopecia. *Indian Journal of Dermatology, Venereology and Leprology* 75: 47–51.

Inui, S., and S. Itami. 2011. Molecular basis of androgenetic alopecia: From androgen to paracrine mediators through dermal papilla. *Journal of Dermatological Science* 61: 1–6.

Inui, S., and S. Itami. 2013. Androgen actions on the human hair follicle: perspectives. *Experimental Dermatology* 22: 168–171.

Jepps, O.G., Y. Dancik, Y.G. Anissimov, and M.S. Roberts. 2013. Modeling the human skin barrier: Towards a better understanding of dermal absorption. *Advanced Drug Delivery Reviews* 65: 152–168.

Kulkarni, C.V., W. Wachter, G. Iglesias-Salto, W. Engelskirchen, and S. Ahualli. 2011. Monoolein: a magic lipid? *Physical Chemistry Chemical Physics: PCCP* 13: 3004–3021.

Lapteva, M., and Y.N. Kalia. 2013. Microstructured bicontinuous phase formulations: their characterization and application in dermal and transdermal drug delivery. *Expert opinion on drug delivery* 10: 1043–1059.

Liu, H., S. Chen, Y. Zhou, X. Che, Z. Bao, S. Li, and J. Xu. 2013. The effect of surface charge of glycerol monooleate-based nanoparticles on the round window membrane permeability and cochlear distribution. *Journal of Drug Targeting* 21: 846–854.

Madheswaran, T., R. Baskaran, R.K. Thapa, J.Y. Rhyu, H.Y. Choi, J.O. Kim, C.S. Yong, and B.K. Yoo. 2013a. Design and in vitro evaluation of finasteride-loaded liquid crystalline nanoparticles for topical delivery. *AAPS PharmSciTech* 14: 45–52.

Madheswaran, T., R. Baskaran, C.S. Yong, and B.K. Yoo. 2013b. Enhanced topical delivery of finasteride using glyceryl monooleate-based liquid crystalline nanoparticles stabilized by cremophor surfactants. *AAPS PharmSciTech* 15: 44–51.

Mulet, X., B.J. Boyd, and C.J. Drummond. 2013. Advances in drug delivery and medical imaging using colloidal lyotropic liquid crystalline dispersions. *Journal of Colloid and Interface Science* 393: 1–20.

Murgia, S., A.M. Falchi, M. Mano, S. Lampis, R. Angius, A.M. Carnerup, J. Schmidt, G. Diaz, M. Giacca, and Y. Talmon. 2010. Nanoparticles from lipid-based liquid crystals: emulsifier influence on morphology and cytotoxicity. *Journal of Physical Chemistry B* 114: 3518–3525.

Mysore, V. 2012. Finasteride and sexual side effects. *Indian Dermatology Online Journal* 3: 62–65.

Park, S.H., B.B. Das, F. Casagrande, Y. Tian, H.J. Nothnagel, M. Chu, H. Kiefer, K. Maier, A.A. De Angelis, and F.M. Marassi. 2012. Structure of the chemokine receptor CXCR1 in phospholipid bilayers. *Nature* 491: 779–783.

Prow, T.W., J.E. Grice, L.L. Lin, R. Faye, M. Butler, W. Becker, E.M.T. Wurm, C. Yoong, T.A. Robertson, H.P. Soyer, and M.S. Roberts. 2011. Nanoparticles and microparticles for skin drug delivery. *Advanced Drug Delivery Reviews* 63: 470–491.

Ridolfi, D.M., P.D. Marcato, G.Z. Justo, L. Cordi, D. Machado, and N. Durán. 2012. Chitosan-solid lipid nanoparticles as carriers for topical delivery of tretinoin. *Colloids and Surfaces B: Biointerfaces* 93: 36–40.

Rojanasakul, Y., L.Y. Wang, M. Bhat, D.D. Glover, C.J. Malanga, and J.K. Ma. 1992. The transport barrier of epithelia: a comparative study on membrane permeability and charge selectivity in the rabbit. *Pharmaceutical Research* 9: 1029–1034.

Svensson, O., K. Thuresson, and T. Arnebrant. 2008. Interactions between chitosan-modified particles and mucin-coated surfaces. *Journal of Colloid and Interface Science* 325: 346–350.

de Valente Duarte Sousa, I.C., and A. Tosti. 2013. New investigational drugs for androgenetic alopecia. *Expert Opinion on Investigational Drugs* 22: 573–589.

Van Neste, D., V. Fuh, P. Sanchez-Pedreno, E. Lopez-Bran, H. Wolff, D. Whiting, J. Roberts, D. Kopera, J.J. Stene, S. Calvieri, A. Tosti, E. Prens, M. Guarrera, P. Kanojia, W. He, and K.D. Kaufman. 2000. Finasteride increases anagen hair in men with androgenetic alopecia. *British Journal of Dermatology* 143: 804–810.

Piemi, Youenang. 1999. M. P., Korner, D., Benita, S., and Marty, J. P., Positively and negatively charged submicron emulsions for enhanced topical delivery of antifungal drugs. *Journal of Controlled Release* 58: 177–187.

Zhang, J., and B. Michniak-Kohn. 2011. Investigation of microemulsion microstructures and their relationship to transdermal permeation of model drugs: ketoprofen, lidocaine, and caffeine. *International Journal of Pharmaceutics* 421: 34–44.